10 Years of Higgs Boson Measurements at ATLAS and CMS

Kerstin Tackmann[1,2]

[1]*Deutsches Elektronen-Synchrotron DESY, Notkestr. 85, 22607 Hamburg, Germany*
[2]*Institut für Experimentalphysik, Universität Hamburg, Luruper Chaussee 149, 22761 Hamburg, Germany*

Abstract

In the summer of 2012, the ATLAS and CMS experiments at the Large Hadron Collider announced the discovery of a new particle, with properties consistent with those expected from the Standard Model Higgs boson. Since then, its properties and its interactions with other particles have been studied by both experiments using the data that have been collected in the meantime, increasing the number of Higgs bosons produced by a factor of 36. This article gives a brief overview of the measurement of the Higgs boson mass and of Higgs boson interactions with gauge bosons and with third-generation fermions. To date, all measurements have been found to be consistent with the predictions of the Standard Model of particle physics.

1. INTRODUCTION

The tenth anniversary of the Higgs boson discovery in the summer of 2012 is a good opportunity to look back at the discovery and at what has been learned about the nature of the Higgs boson in those ten years. The discovery itself had really been a textbook discovery, with an excess of events compatible with a Higgs boson mass of around 125 GeV slowly emerging at both experiments as the size of the analyzed dataset grew. In the summer of 2012, the statistical significance of the excess reached or surpassed 5σ at both experiments [1, 2], and the news of the discovery was met with large excitement. A new particle had been observed. But what was this new particle?

The Standard Model of particle physics (SM) makes very clear predictions about the properties of the SM Higgs boson [3, 4, 5, 6, 7, 8, 9, 10, 11, 12]. It is an elementary particle, and it is a scalar, or in other words, it has a spin of 0. The strength of its interactions with other particles is directly related to that particle's mass. This makes the Yukawa interaction between the Higgs boson and the fermions the only interaction in the SM that distinguishes between the three fermion generations. It also predicts Higgs boson self-interactions with a strength related to its vacuum expectation value. In contrast to many extensions of the SM, the SM only predicts the existence of a single Higgs boson.

The SM does not predict the mass of the Higgs boson, but for any given mass, it predicts the cross sections for all Higgs boson production processes and the decay rates for all Higgs boson decay channels. At the time the ATLAS [13] and CMS [14] experiments at the Large Hadron Collider (LHC) [15] started to collect data in 2010, the Higgs boson mass was the only unknown parameter of the SM needed to predict the production cross sections and decay rates. Results from experiments at the LEP, SLD, and Tevatron colliders constrained the mass of a potential SM Higgs boson to be between 114 and 158 GeV or above 175 GeV [16].

The discovery was the starting point of the in-depth investigation of the properties of this new particle to first determine whether or not it is compatible with being a Higgs boson, and to determine its properties to check their compatibility with the predictions of the SM and of extended models.

This article gives a brief overview of the measurement of the Higgs boson mass and of Higgs boson interactions with gauge bosons and third-generation fermions, following [17]. A companion article [18] covers studies of the particle's spin, its interactions with second-generation fermions as well as Higgs boson self-interactions, and finally the search for other Higgs bosons.
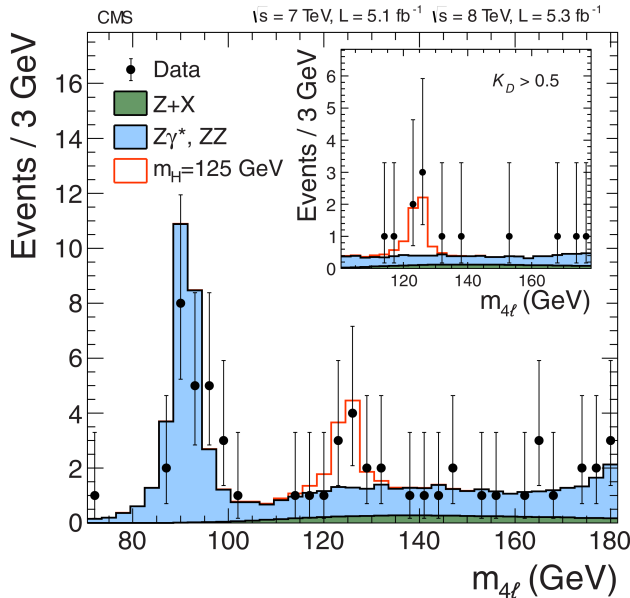
2. HIGGS BOSON MASS

The mass of the Higgs boson, a free parameter in the SM, is a crucial input to predict the production cross sections and the decay rates of the Higgs boson. Before the discovery, cross sections and decay rates had been computed for a wide range of masses to study the feasibility of observing and studying the Higgs boson at the LHC and to provide crucial input to the design of the detectors and the software.

The Higgs boson mass has been measured in the two decay channels with only light leptons and photons in the final state, which have an excellent invariant mass resolution, as shown for $H \rightarrow \gamma\gamma$ and $H \rightarrow ZZ^* \rightarrow 4\ell$ in Figures 1 and 2, respectively. As such, the mass measurement relies on the precise calibration of the energy and momentum measurements of the ATLAS and CMS tracking detectors, muon systems, and electromagnetic calorimeters.

This measurement was the first precision measurement at the LHC: sub-% level precision was reached only two years after the discovery [19, 20]. A statistical combination of the ATLAS and CMS measurements based on the data taken during LHC Run1 reached a precision of 0.19% [21]. Recent measurements achieved a precision of 0.11% based on data taken during Run1 and 2016 using $H \rightarrow ZZ^* \rightarrow 4\ell$ and $H \rightarrow \gamma\gamma$ decays at CMS [22] and 0.14% based on almost the full data taken during Run1 and Run2 using $H \rightarrow ZZ^* \rightarrow 4\ell$ decays at ATLAS [23]. The uncertainties still have a large statistical component, so that the precision of the measurements can be improved further with larger datasets.
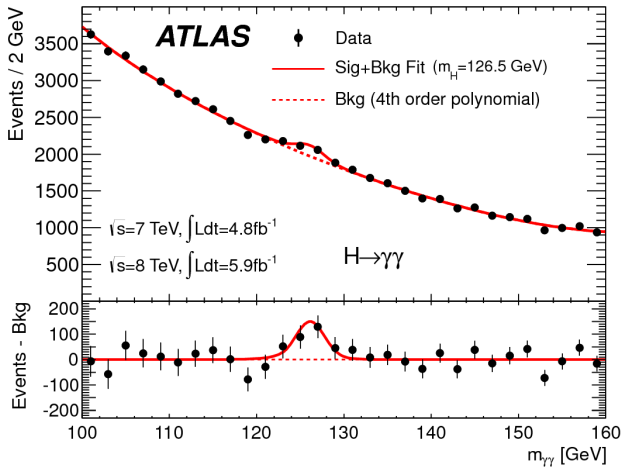
FIGURE 1: Invariant mass of selected diphoton events at the time of the Higgs boson discovery. The signal peak is visible on top of the smoothly falling background, both parametrized by analytical functions. The figure was reproduced from [1]. Similar results were obtained by CMS [2].

FIGURE 2: Invariant mass of selected events with four light leptons at the time of the Higgs boson discovery. The main background is estimated from the simulation, and the signal is clearly visible. The peak from $pp \to Z \to 4\ell$ around 90 GeV serves as an important cross-check of the analysis. The figure was reproduced from [2]. Similar results were obtained by AT-LAS [1].

3. HIGGS BOSON PRODUCTION AND DECAYS AT LHC

Several processes are predicted to contribute to the production of Higgs bosons in proton-proton collisions. According to the SM, the dominant process is gluon fusion, accounting for 88% of the Higgs boson production cross section for pp collisions at 13 TeV for a Higgs boson with a mass of 125 GeV. The gluon fusion process proceeds via a triangular fermion loop, expected to be dominated by the top quark contributions. Vec-

tor boson fusion, which has a distinct signature with two well-separated hadronic jets and little hadronic activity between them, accounts for about 7% of Higgs boson production in the SM. Associated production with a vector boson (W or Z) accounts for about 4% of the production cross section and has a clear signature with the vector boson reconstructed in leptonic or hadronic decays. Finally, associated production with a $t\bar{t}$ pair can be tagged by the presence of the $t\bar{t}$ decay products and accounts for about 1% of the production cross section in the SM.

The rate of Higgs boson production is many orders of magnitude smaller than that of other processes such as the production of hadronic final states via the strong interaction, the production of weak vector bosons, or the production of $t\bar{t}$ pairs. Many of these processes are important backgrounds for Higgs boson measurements and searches. Extracting the Higgs signal from the overwhelming backgrounds requires a careful design of the triggers, the event selections, and the background estimation.

The accessible Higgs boson decay channels depend quite strongly on the Higgs boson mass. For a mass of 125 GeV, a large variety of decay channels is accessible, allowing for very detailed studies of the Higgs boson properties. The decays to two photons, $H \to \gamma\gamma$, to two τ leptons, $H \to \tau\tau$, and to a $b\bar{b}$ pair, $H \to b\bar{b}$, which would be the primary discovery channels for a lighter Higgs boson, are still sufficiently large at 125 GeV. On the other hand, the decays to two vector bosons, $H \to WW^*$ and $H \to ZZ^*$, which would be the dominant decay channels for a heavier Higgs boson, are already accessible in leptonic vector boson decays with one of the vector bosons being off-shell. Table 1 shows the number of Higgs boson decays expected to be produced and selected in the five main Higgs boson decay channels for a mass of 125 GeV per fb^{-1} in pp collisions at 13 TeV. Considering the quite small number of selected events and taking into account the presence of sizeable backgrounds, quite large datasets are needed for precision measurements.

	Produced	Selected
$H \to \gamma\gamma$	130	46
$H \to ZZ^*$	1400 (7)	1.5
$H \to WW^*$	12000 (280)	42
$H \to \tau\tau$	3500	17
$H \to b\bar{b}$	32000	66

TABLE 1: Number of Higgs bosons produced and selected in the five main decay channels per fb^{-1} at a collision energy of 13 TeV [24]. The numbers in parentheses take into account the branching fractions of $Z \to \ell\ell$ and $W \to \ell\nu$ ($\ell = e, \mu$).

An overview of Higgs boson production and decays along with references to the original literature can be found in [25].

4. HIGGS BOSON DECAYS TO GAUGE BOSONS

The observation of the Higgs boson was driven by its decays to gauge boson pairs, two photons, two Z bosons, and two W

bosons. For the latter, their decays to light charged leptons (*e*, *µ*) and neutrinos were exploited.

4.1. Higgs Decays to Two Photons

The $H \rightarrow \gamma\gamma$ decay has only a tiny expected branching fraction of about 0.2% and therefore only a very small signal yield. On the other hand, the fairly simple final state of two photons can be selected with high efficiency (see Table 1). The backgrounds for the diphoton signature are very large. The suppression of hadronic backgrounds, where a light meson decay such as $\pi^0 \rightarrow \gamma\gamma$ mimic a single photon, requires suppression factors of several 10^3. This is achieved thanks to the granular electromagnetic calorimeters, allowing a quite detailed measurement of the shape of energy deposits. These are wider and less isolated for the case of photons from neutral meson decays, which typically leave a single energy deposit. After the event selection, the remaining background is dominated by events with two photons produced nonresonantly, accounting for roughly 75% of the background. The expected signal purity in the invariant mass range where the signal is located is about 3%.

The excellent invariant mass resolution of the photon pair, which can be as good as 1.4 GeV [1], results in a clear peak on top of a smoothly falling background (see Figure 1), allowing a robust background subtraction.

4.2. Higgs Decays to Two Z Bosons

The signal yield of the $H \rightarrow ZZ^* \rightarrow 4\ell$ decay is expected to be tiny for a Higgs boson of 125 GeV. While the $H \rightarrow ZZ^*$ branching fraction is sizeable, about 2.6%, the small $Z \rightarrow \ell\ell$ branching fraction combined with the experimental efficiencies results in only 7.5 expected signal events in the data set used for the Higgs boson discovery [2]. The leptons originating from the off-shell Z^* boson tend to have low momenta, with their momentum distributions peaking below 10 and 20 GeV, respectively. The reconstruction and the background suppression for the low-momentum electrons are among the experimental challenges for this final state.

The small number of background events, mostly from nonresonant ZZ^* production, and the excellent invariant mass resolution of about 1-2% in this final state still result in a very clean signal peak with a signal-to-background ratio of about 2 as can be seen in Figure 2.

4.3. Higgs Decays to Two W Bosons

The $H \rightarrow WW^* \rightarrow e\nu\mu\nu$ decay has a significantly larger signal yield than the $H \rightarrow ZZ^* \rightarrow 4\ell$ decay, thanks to the quite large $H \rightarrow WW^*$ branching ratio of about 21.5% for a Higgs boson with a mass of 125 GeV. About 25 signal events were expected to be selected with zero or one hadronic jet in the event in addition to the Higgs boson decay products, considering the transverse mass range between 93.75 and 125 GeV [1].

The presence of neutrinos in the final state results in a significantly worse mass resolution compared to $H \rightarrow \gamma\gamma$ and $H \rightarrow ZZ^* \rightarrow 4\ell$ decays and motivates the use of the transverse mass, computed from the transverse energy and momentum components of the system of the two leptons and the missing momentum.

The $e\nu\mu\nu$ signature is affected by large backgrounds, visible in Figure 3 for events with zero or one hadronic jet in the final
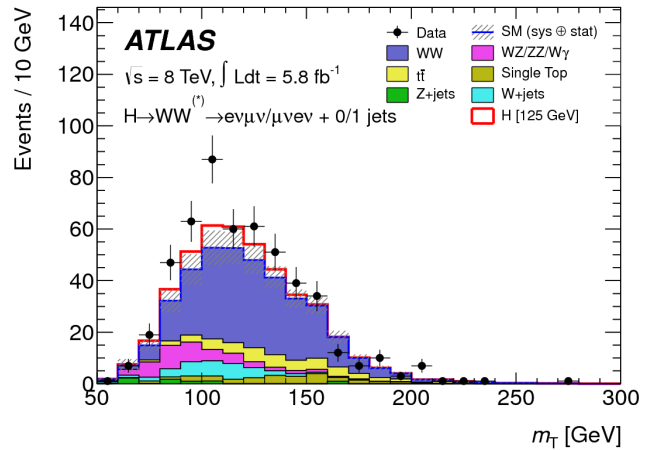
FIGURE 3: Transverse mass distribution of $H \rightarrow WW^* \rightarrow e\nu\mu\nu$ candidate events with zero or one hadronic jet in the event at the time of the Higgs boson discovery. The signal is visible as excess compared to the estimated backgrounds. The figure was reproduced from [1]. Similar results were obtained by CMS [2].

state. The large backgrounds from nonresonant WW^* and from $t\bar{t}$ production as well as the smaller, but difficult, background from W+jet production are estimated from dedicated control samples.

5. HIGHLIGHTS OF RUN1

The discovery of the Higgs boson in the summer of 2012 rested mainly on the statistical combination of the results in the three decay channels discussed above, reaching a significance of 6.0σ (4.9σ expected) [1] and 5.0σ (5.8σ expected) [2] by the two experiments, respectively. The three decay channels were observed separately with a significance of above 5σ shortly afterward. At the end of Run1, using the full dataset taken in 2011 and 2012, the global signal strength μ was measured to be $1.33^{+0.21}_{-0.18}$, i.e., with a precision of about 15% [26]. In a given decay channel, $\mu = N_{meas}/N_{SM}$, where N_{meas} is the number of measured Higgs boson events, while N_{SM} is the number predicted by the SM. The global signal strength μ is measured in all decay channels simultaneously, testing the global compatibility of the data with the SM.

The Run1 dataset was also used for more detailed studies of the properties of the Higgs boson, such as determinations of its couplings to the other particles. Couplings are often measured in terms of coupling strengths modifiers κ, which are multiplicative parameters to the SM coupling in the Lagrangian, modifying the overall strength of the coupling. Hence, a measurement compatible with $\kappa = 1$ means that the measured coupling is consistent with the prediction of the SM. As example, Figure 4 shows the coupling strength modifiers for Higgs couplings to vector bosons and to fermions (assumed to be the same for all vector bosons and for all fermions, respectively), constrained from the single decay channels to vector bosons and their statistical combination. Sensitivity to the coupling strength to fermions comes mainly from the gluon fusion fermion loop. The results are compatible with the SM. One important conclusion that could be drawn from the early results was the exclusion of the existence of a heavy, SM-like, fourth

generation of fermions, which would result in a sizeable increase in the Higgs production cross section. This was ruled out by the data.
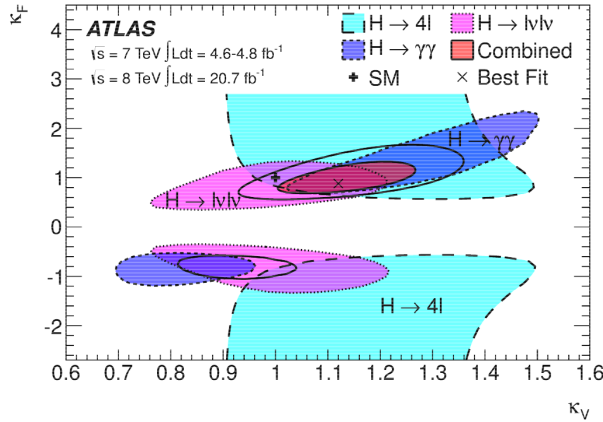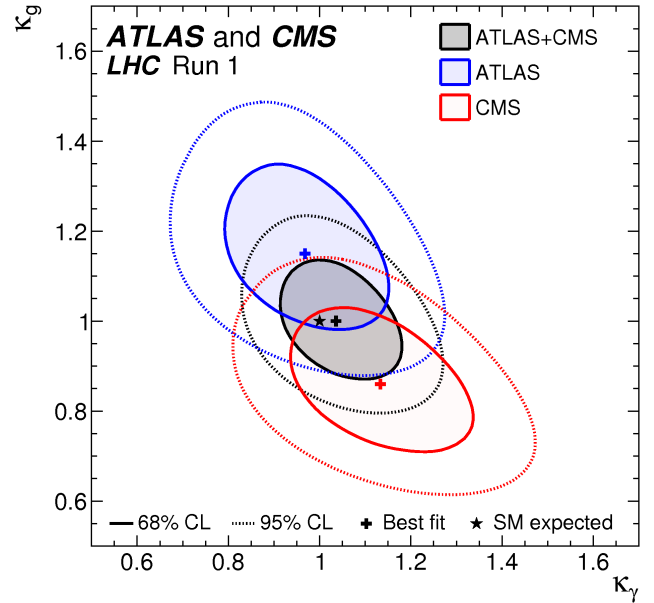

FIGURE 4: Coupling strength modifiers for Higgs couplings to vector bosons and to fermions determined from several Higgs decay channels and their statistical combination. The figure was reproduced from [26].

The existence of two experiments with similar goals, but employing very different detector technologies, working independently, was indispensable to cross-check each other's results. The most precise results from the Run1 dataset were obtained by a statistical combination of the results of both experiments. The combination included all main decay channels. A precision of 10% was reached for the global signal strength, $\mu = 1.09 \pm 0.11$ [27]. The combination allowed the observation of Higgs production through the vector boson fusion process, as well as Higgs boson decays into two τ leptons, $H \rightarrow \tau\tau$ (see also Section 6.1), each with a significance of more than 5σ. Figure 5 shows the constraints on the coupling strength modifiers for effective Higgs couplings to photons and to gluons obtained from the separate experiments and their statistical combination. In the SM, these couplings proceed via fermion and vector boson loops but are assumed to be effective, point-like couplings for the purpose of this study.

6. HIGGS BOSON COUPLINGS TO FERMIONS

The Yukawa couplings between the Higgs boson and the fermions play a special role in the SM. The mechanism of electroweak symmetry breaking does not require any coupling between the Higgs boson and the fermions. Instead, the Yukawa couplings are added to the model to explain the masses of the charged fermions. The large fermion mass hierarchy translates to an expected large hierarchy in the strength of the Yukawa couplings, which led to the expectation that the interactions with the third generation of fermions should be observed first.

Higgs boson production processes and decays directly and indirectly sensitive to Higgs boson couplings to fermions had been investigated in Run1, and two important conclusions had been obtained: first, the existence of Higgs Yukawa couplings was inferred from the good compatibility of the measured Higgs boson production with that predicted by the SM, which is dominated by the gluon fusion process, and second,

FIGURE 5: Coupling strength modifiers for Higgs couplings to photons and to gluons determined by the separate experiments and their statistical combination. The figure was reproduced from [27].

the $H \rightarrow \tau\tau$ decay was observed in the combination of the results of both experiments. The much larger dataset collected during Run2 made the direct study of Higgs boson couplings to fermions particularly interesting.

6.1. Higgs Couplings to τ Leptons

While the $H \rightarrow \tau\tau$ final state contains neutrinos, in contrast to the $H \rightarrow WW^*$ final state, their impact on the invariant mass resolution is mitigated by the small mass of the τ, causing the neutrinos to be almost collinear with the visible τ decay products. This can be used to construct estimators of the di-τ invariant mass with improved resolution.

The large $Z \rightarrow \tau\tau$ backgrounds are reduced by selecting regions of phase space in which $H \rightarrow \tau\tau$ is enhanced relative to $Z \rightarrow \tau\tau$: with large transverse momentum of the di-τ pair, typically of the order of 100 GeV and above, or with vector boson fusion topology. The $H \rightarrow \tau\tau$ signal is visible as an excess in the invariant di-τ mass distribution on the shoulder of the $Z \rightarrow \tau\tau$ peak (see Figure 6).

The $H \rightarrow \tau\tau$ decay was observed with a significance of more than 5σ by both experiments separately with the data taken between 2011 and 2016. This observation constituted the first (single-experiment) direct observation of Higgs Yukawa couplings to fermions.

6.2. Higgs Couplings to Top Quarks

Being the heaviest known particle, the coupling of the top quark to the Higgs boson is expected to be strong, and its direct observation through Higgs boson production in association with a $t\bar{t}$ pair was of high interest. With the decay products of the $t\bar{t}$ pair and the Higgs boson, this process has a challenging final state with high multiplicity, as can be appreciated in the event display shown in Figure 7.
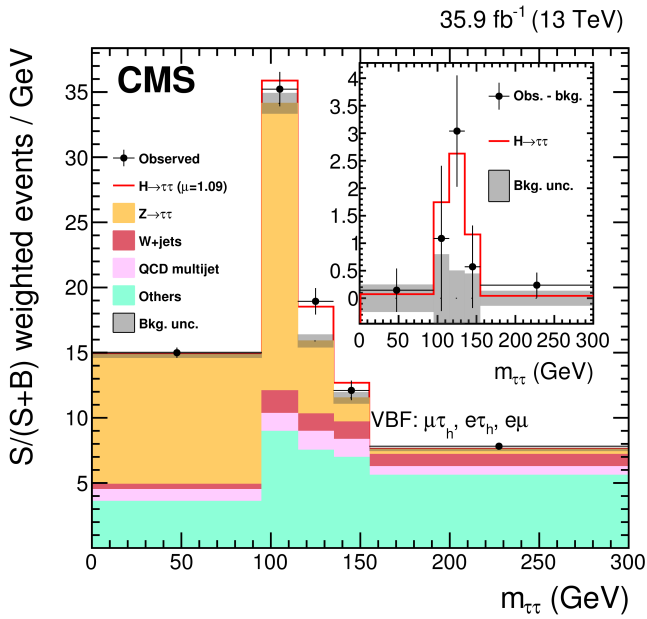
FIGURE 6: Invariant mass distribution of $H \to \tau\tau$ candidate events with event topology consistent with Higgs boson production through vector boson fusion in the dataset collected in 2016. The inset shows the data after background subtraction. The figure was reproduced from [28]. Similar results were obtained by ATLAS [29].
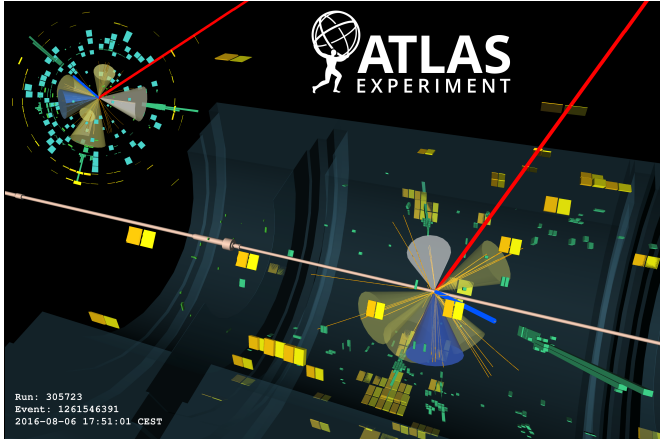
FIGURE 7: $t\bar{t}H$ candidate event containing a muon candidate (red track), an electron candidate (blue track and green bars), a candidate of a hadronically decaying τ (grey cone), and multiple hadronic jets (blue and yellow cones). The hadronic jet indicated by the blue cone is tagged to contain a b-quark. The figure was reproduced from [30].

The $t\bar{t}H$ production process was initially observed by combining the results in several Higgs boson decay channels, including $H \to \gamma\gamma$, $H \to ZZ^*$, $H \to WW^*$, $H \to \tau\tau$, and $H \to b\bar{b}$, using the data collected between 2011 and 2016 (or 2017, respectively) [35, 36]. The decay channels with larger branching fractions suffer from large and difficult backgrounds. For the $t\bar{t}H(\to b\bar{b})$ process, a particular challenge lies in the modeling of the experimentally not well constrained $t\bar{t}b\bar{b}$ process. To increase the efficiency of the event selection, rather than targeting the $H \to ZZ^*$, $H \to WW^*$, and $H \to \tau\tau$ decays separately,

an analysis selecting final states with multiple charged leptons, including light leptons and τs, targets these three decays together.[1] A particular experimental challenge is the estimation of backgrounds with other objects misidentified as leptons.

$t\bar{t}H$ production also was observed in the $H \to \gamma\gamma$ decay channel alone by using the data collected between 2015 (or 2016, respectively) and 2018 [31, 32] (see Figure 8).

6.3. Higgs Couplings to b Quarks

The $H \to b\bar{b}$ decay is the decay with the largest branching fraction; the SM predicts it to be about 58%. The $b\bar{b}$ final state has however very large backgrounds in particular from strong production of hadronic final states including b quarks. These can be reduced by focusing on Higgs boson production in association with a vector boson V, VH, with V decaying to final states with light leptons ($Z \to \ell\ell$, $Z \to \nu\nu$, $W \to \ell\nu$ with $\ell = e, \mu$). The light leptons also provide a clear signature for the trigger. In turn, thanks to the large branching fraction, $H \to b\bar{b}$ is the best decay channel to observe VH production.

Combining the results from the search for $H \to b\bar{b}$ in VH production with analyses targeting other production processes, the $H \to b\bar{b}$ decay was observed with a significance of more than 5σ using data collected between 2011 and 2017 [33, 34], completing the direct observation of Higgs boson couplings to third-generation fermions. Given the large branching fraction, this observation also constrains beyond Standard Model contributions to the total Higgs width.

In addition, a combination of the $VH(\to b\bar{b})$ search with analyses targeting other Higgs boson decay channels, VH production was observed with a significance of more than 5σ on the same dataset [33].
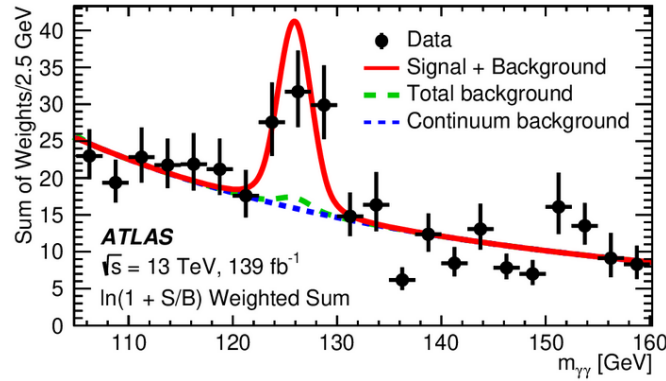
7. HIGGS BOSON WIDTH

Measurements at the LHC always constrain the product of the Higgs boson production cross section and decay branching fractions. Separate determinations of these quantities require an assumption on the Higgs boson width. The total width predicted by the Standard Model of 4.1 MeV is too small to be measured directly at the LHC. It can however be constrained indirectly from the study of off-shell Higgs boson production [37, 38, 39], e.g., studying Higgs boson production in $H \to ZZ$ decays with $m_{ZZ} > 2m_Z$, with both Z bosons on-shell (see Figure 10). The assumption that the couplings are the same for on-shell and off-shell Higgs bosons allows one to constrain the Higgs boson width via $\mu_{\text{off-shell}} = \Gamma_H / \Gamma_{H,\text{SM}} \times \mu_{\text{on-shell}}$, where $\mu_{\text{off-/on-shell}}$ are the signal strengths measured off- and on-shell, respectively. Using data collected in 2016 and 2017, the first evidence for Higgs boson off-shell production was obtained with a significance of 3.6σ. The Higgs boson width was determined to be $\Gamma_H = 3.2^{+2.4}_{-1.7}$ MeV [40].

8. COUPLINGS AND DIFFERENTIAL MEASUREMENTS AT THE END OF RUN2

Ten years after the Higgs boson discovery, the five main production processes, gluon fusion, vector boson fusion, and asso-

---

[1]An exception is $H \to ZZ^* \to 4\ell$, which is excluded and targeted separately.

FIGURE 8: Invariant mass of diphoton candidate events selected in 20 event categories compatible with Higgs boson production in association with a $t\bar{t}$ pair. Each event is weighted by $\ln(1 + S/B)$, where S and B are fitted signal and background yields in the respective event category the event falls into. The figure was reproduced from [31]. Similar results were obtained by CMS [32].
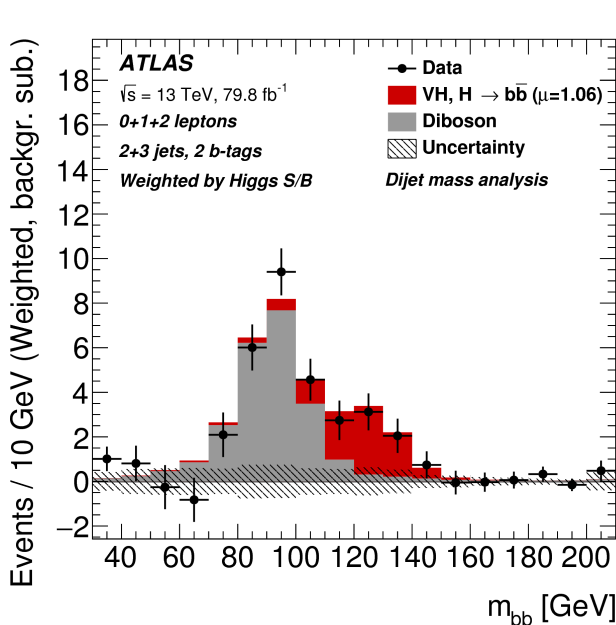

FIGURE 9: Invariant mass distribution of the $b\bar{b}$ pair after subtraction of all backgrounds apart from the $VZ(\rightarrow b\bar{b})$ background, which also serves as a control channel. Each event is weighted by S/B, where S and B are the fitted background and signal yield in the respective event category the event falls into. The figure was reproduced from [33]. Similar results were obtained by CMS [34].

ciated production with a W boson, with a Z boson, and with a $t\bar{t}$ pair, and the five main decay channels, $H \rightarrow \gamma\gamma$, $H \rightarrow ZZ^*$, $H \rightarrow WW^*$, $H \rightarrow \tau\tau$, and $H \rightarrow b\bar{b}$, have been observed and are used to make detailed measurements of the properties of the Higgs boson and its interactions. The signal strength measurements for 30 combinations of production processes and decay channels are presented in Figure 11, including also the $H \rightarrow \mu\mu$ and $H \rightarrow Z\gamma$ decay channels, which have not yet been observed. All measurements are in good agreement with the predictions of the SM. The global signal strength, taking into account all production processes and decay channels, has been measured to be $\mu = 1.05 \pm 0.06$ [43] and $\mu = 1.00 \pm 0.06$ [42] by the ATLAS and CMS collaborations, respectively.
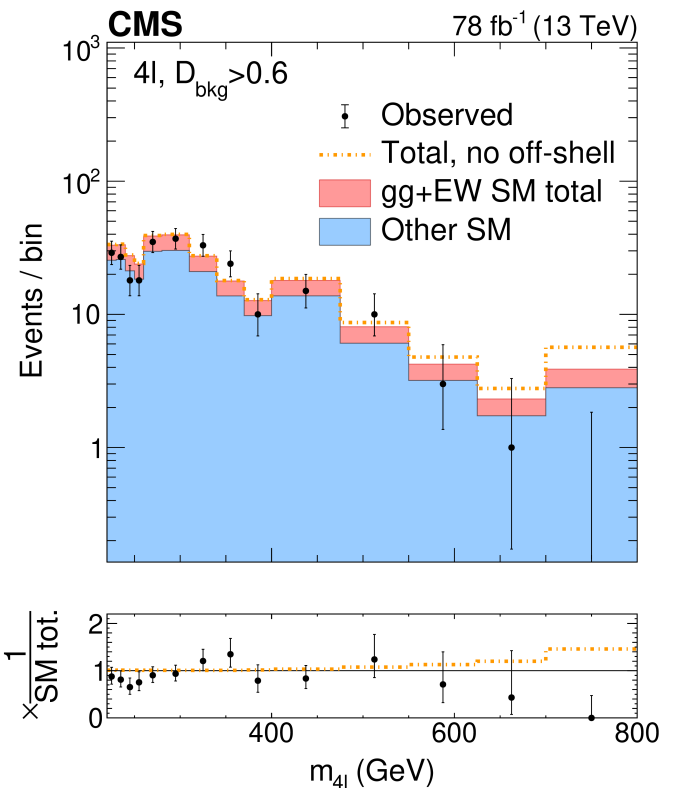
FIGURE 10: Invariant mass of the four-lepton system in a wide range including the region of off-shell Higgs boson production. The dotted line shows the predicted distribution in the case of no off-shell Higgs boson production. The figure was reproduced from [40]. Similar results were obtained by ATLAS [41].

The SM predicts a clear correlation between the mass of an elementary particle and its coupling to the Higgs boson. The compatibility of the data with that prediction is depicted in Figure 12, under the assumption that there are no contributions to the total width beyond those predicted by the SM. After the observation of Higgs couplings to third-generation fermions, the observation and measurement of Higgs couplings to second-generation fermions are now of particular interest (see also [18]).
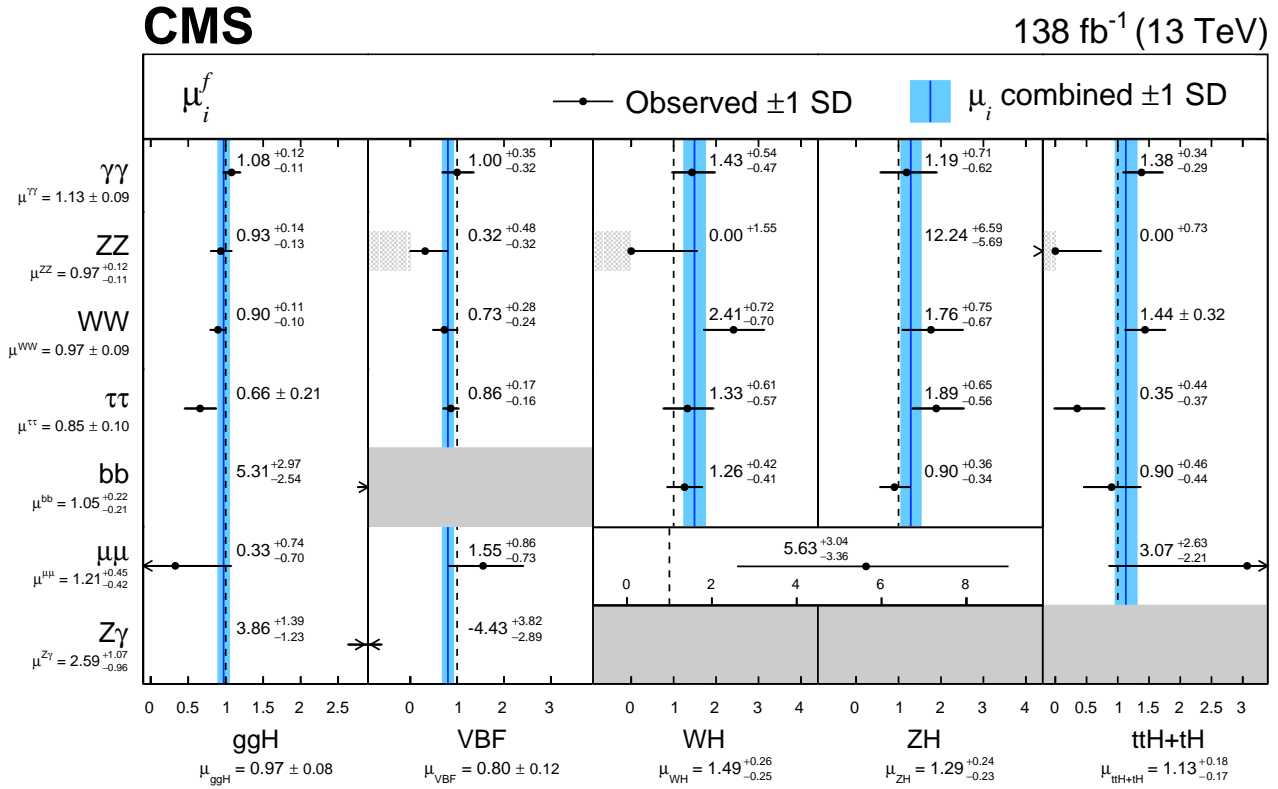
FIGURE 11: Signal strengths of 30 combinations of Higgs boson production processes and decay channels. The figure was reproduced from [42]. Similar results were obtained by ATLAS [43].

With the increased size of the available dataset, a more detailed study of the kinematics in Higgs production and decays becomes possible. This is of particular interest since the effects of physics beyond the SM can be enhanced in certain regions of phase space, such as tails of kinematic distributions. The kinematics are studied by measuring cross sections in a variety of kinematic regions for each of the main production processes as shown in Figure 13. The kinematic regions have been defined to maximize the sensitivity to physics beyond the SM, while limiting the model dependence in the measurements. Within the current uncertainties, all measurements are compatible with the predictions of the SM.

9. CONCLUSIONS

The understanding of the Higgs boson and its interactions has come a long way since its discovery in the summer of 2012. The main production processes and decay channels have been observed and the precision with which the couplings of the Higgs boson are measured has increased significantly, as can be seen in Figure 14. This was made possible by the very large increase in the amount of data collected and analyzed—the number of Higgs bosons produced at the LHC increased by a factor of 36 during the ten years since the Higgs boson discovery—but also by improvements in the detector performance and calibration, data reconstruction, and analysis techniques. So far, all measurements are consistent with the predictions of the SM. The next step in precision will be reached with a statistical combination of the Run2 results from ATLAS and CMS.
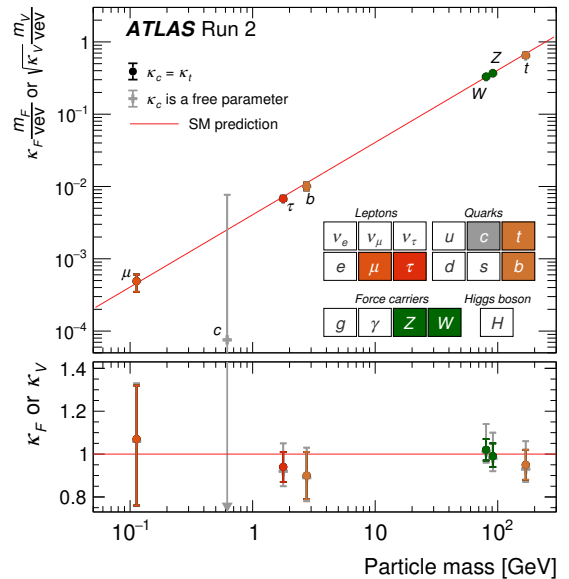
FIGURE 12: Coupling strengths of gauge bosons and fermions to the Higgs boson as a function of the particle's mass. The figure was reproduced from [43]. Similar results were obtained by CMS [42].

Many scenarios beyond the SM predict only percent-level deviations from the SM, requiring much more precise measure-
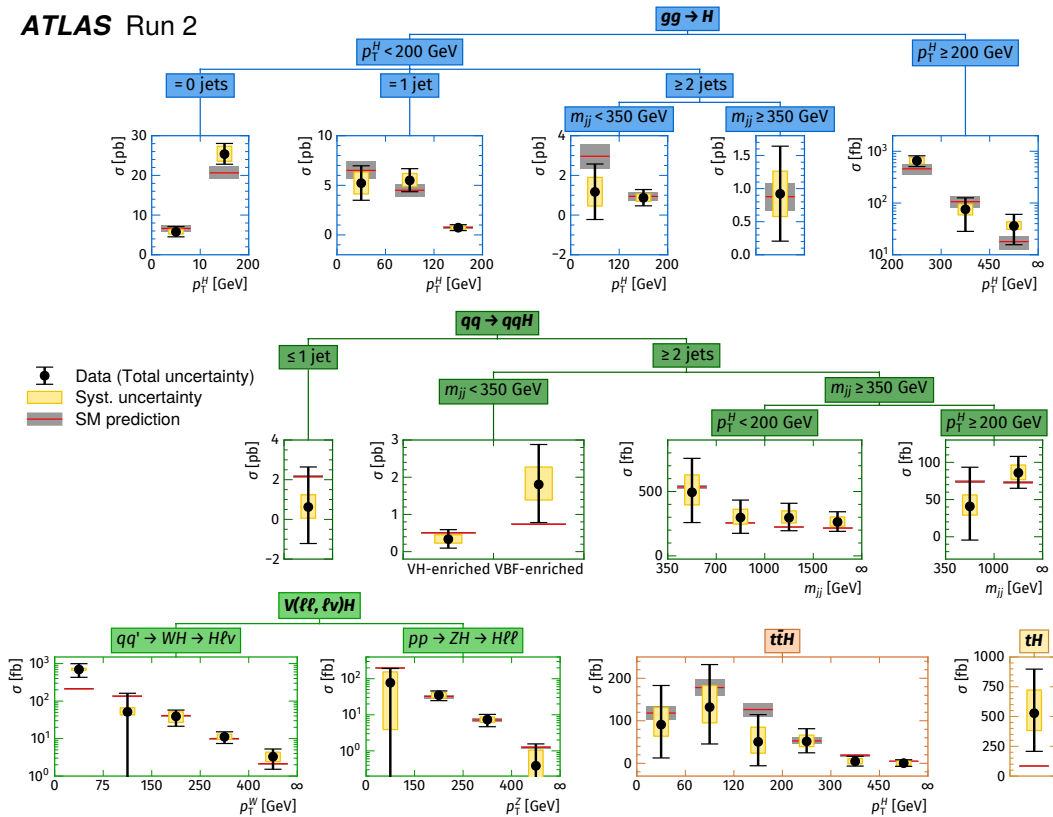
FIGURE 13: Cross sections measured in several kinematic regions for each of the main production processes. The figure was reproduced from [43].
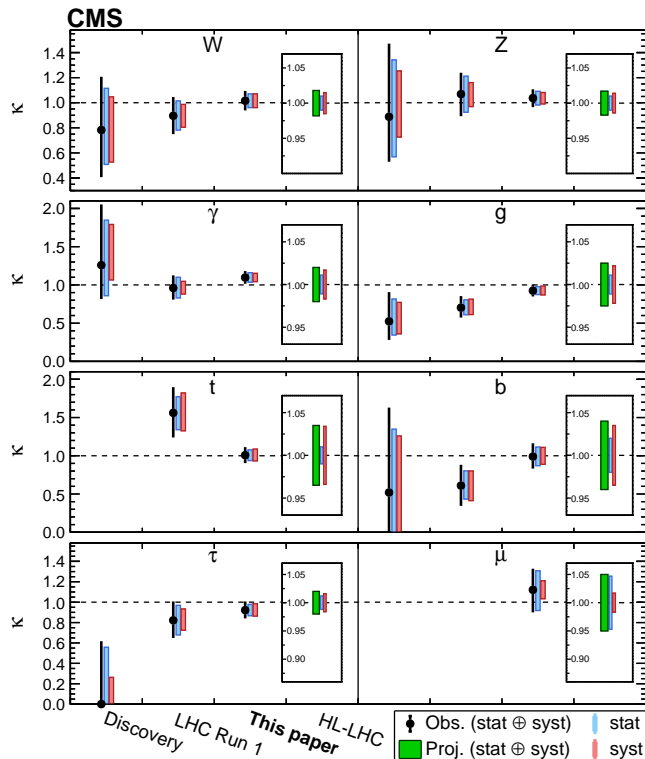

FIGURE 14: Coupling strengths of gauge bosons and fermions to the Higgs boson at the time of the Higgs boson discovery, using the data collected in Run1, ten years after the Higgs boson discovery, and the precision projected for High-Luminosity LHC. The figure was reproduced from [42].

ments of the Higgs boson couplings than available today. Despite the big steps that have been taken in understanding the properties of the Higgs boson, we are just at the beginning of this exciting journey. Run3 and the High-Luminosity LHC are ahead, and the much harsher experimental conditions expected at High-Luminosity LHC require upgrades of the detectors and the work for these is in full swing. The data to be collected is expected to increase the number of Higgs bosons by another factor of 20, allowing for much more detailed studies of the Higgs boson properties (see, e.g., Figure 14). Higgs boson studies promise to remain exciting over the next decades!

CONFLICTS OF INTEREST

The author declares that there are no conflicts of interest regarding the publication of this paper.

ACKNOWLEDGMENTS

References

[1] ATLAS Collaboration, G. Aad et al., "Observation of a new particle in the search for the Standard Model Higgs boson with the ATLAS detector at the LHC," *Phys. Lett. B* **716** (2012) 1–29, arXiv:1207.7214 [hep-ex].

[2] CMS Collaboration, S. Chatrchyan et al., "Observation of a New Boson at a Mass of 125 GeV with the CMS Experiment at the LHC," *Phys. Lett. B* **716** (2012) 30–61, arXiv:1207.7235 [hep-ex].

[3] S. L. Glashow, "Partial-symmetries of weak interactions," *Nucl. Phys.* **22** (1961) 579–588.

[4] A. Salam, "Weak and Electromagnetic Interactions," *Conf. Proc. C* **680519** (1968) Proceedings of the eighth Nobel symposium.

[5] S. Weinberg, "A Model of Leptons," *Phys. Rev. Lett.* **19** (1967) 1264–1266.

[6] F. Englert and R. Brout, "Broken Symmetry and the Mass of Gauge Vector Mesons," *Phys. Rev. Lett.* **13** (1964) 321–323.

[7] P. W. Higgs, "Broken symmetries, massless particles and gauge fields," *Phys. Lett.* **12** (1964) 132–133.

[8] P. W. Higgs, "Broken Symmetries and the Masses of Gauge Bosons," *Phys. Rev. Lett.* **13** (1964) 508–509.

[9] P. W. Higgs, "Spontaneous Symmetry Breakdown without Massless Bosons," *Phys. Rev.* **145** (1966) 1156–1163.

[10] G. S. Guralnik, C. R. Hagen, and T. W. B. Kibble, "Global Conservation Laws and Massless Particles," *Phys. Rev. Lett.* **13** (1964) 585–587.

[11] T. W. B. Kibble, "Symmetry Breaking in Non-Abelian Gauge Theories," *Phys. Rev.* **155** (1967) 1554–1561.

[12] G. 't Hooft and M. J. G. Veltman, "Regularization and renormalization of gauge fields," *Nucl. Phys. B* **44** (1972) 189–213.

[13] ATLAS Collaboration, G. Aad et al., "The ATLAS Experiment at the CERN Large Hadron Collider," *JINST* **3** (2008) S08003.

[14] CMS Collaboration, S. Chatrchyan et al., "The CMS Experiment at the CERN LHC," *JINST* **3** (2008) S08004.

[15] L. Evans and P. Bryant, "LHC Machine," *JINST* **3** (2008) S08001.

[16] ALEPH, CDF, D0, DELPHI, L3, OPAL, SLD, LEP Electroweak Working Group, Tevatron Electroweak Working Group, SLD Electroweak, Heavy Flavour Groups Collaboration, "Precision Electroweak Measurements and Constraints on the Standard Model," arXiv:1012.2367 [hep-ex].

[17] ATLAS and CMS Collaborations, K. Tackmann, "10 years of Higgs boson measurements at ATLAS and CMS." 2022. https://indico.cern.ch/event/1135177. 10th anniversary of the Higgs boson discovery.

[18] A. David, "Higgs boson—10 years turning the possible into the known," *LHEP* (2023).

[19] ATLAS Collaboration, G. Aad et al., "Measurement of the Higgs boson mass from the $H \rightarrow \gamma\gamma$ and $H \rightarrow ZZ^* \rightarrow 4\ell$ channels with the ATLAS detector using $25\,\mathrm{fb}^{-1}$ of pp collision data," *Phys. Rev. D* **90** no. 5, (2014) 052004, arXiv:1406.3827 [hep-ex].

[20] CMS Collaboration, V. Khachatryan et al., "Precise determination of the mass of the Higgs boson and tests of compatibility of its couplings with the standard model predictions using proton collisions at 7 and 8 TeV," *Eur. Phys. J. C* **75** no. 5, (2015) 212, arXiv:1412.8662 [hep-ex].

[21] ATLAS, CMS Collaboration, G. Aad et al., "Combined Measurement of the Higgs Boson Mass in pp Collisions at $\sqrt{s}$ = 7 and 8 TeV with the ATLAS and CMS Experiments," *Phys. Rev. Lett.* **114** (2015) 191803, arXiv:1503.07589 [hep-ex].

[22] CMS Collaboration, A. M. Sirunyan et al., "A measurement of the Higgs boson mass in the diphoton decay channel," *Phys. Lett. B* **805** (2020) 135425, arXiv:2002.06398 [hep-ex].

[23] ATLAS Collaboration, "Measurement of the Higgs boson mass in the $H \rightarrow ZZ^* \rightarrow 4\ell$ decay channel using $139\,\mathrm{fb}^{-1}$ of $\sqrt{s}$ = 13 TeV pp collisions recorded by the ATLAS detector at the LHC," arXiv:2207.00320 [hep-ex] *Phys. Lett. B* **843** (2023) 137880.

[24] ATLAS Collaboration, G. Aad et al., "Combined measurements of Higgs boson production and decay using up to $80\,\mathrm{fb}^{-1}$ of proton-proton collision data at $\sqrt{s}$ = 13 TeV collected with the ATLAS experiment," *Phys. Rev. D* **101** no. 1, (2020) 012002, arXiv:1909.02845 [hep-ex].

[25] LHC Higgs Cross Section Working Group Collaboration, D. de Florian et al., "Handbook of LHC Higgs Cross Sections: 4. Deciphering the Nature of the Higgs Sector," arXiv:1610.07922 [hep-ph].

[26] ATLAS Collaboration, G. Aad et al., "Measurements of Higgs boson production and couplings in diboson final states with the ATLAS detector at the LHC," *Phys. Lett. B* **726** (2013) 88–119, arXiv:1307.1427 [hep-ex]. [Erratum: Phys.Lett.B 734, 406–406 (2014)].

[27] ATLAS, CMS Collaboration, G. Aad et al., "Measurements of the Higgs boson production and decay rates and con-

straints on its couplings from a combined ATLAS and CMS analysis of the LHC pp collision data at $\sqrt{s} = 7$ and 8 TeV," *JHEP* **08** (2016) 045, `arXiv:1606.02266 [hep-ex]`.

[28] CMS Collaboration, A. M. Sirunyan et al., "Observation of the Higgs boson decay to a pair of τ leptons with the CMS detector," *Phys. Lett. B* **779** (2018) 283–316, `arXiv:1708.00373 [hep-ex]`.

[29] ATLAS Collaboration, M. Aaboud et al., "Cross-section measurements of the Higgs boson decaying into a pair of τ-leptons in proton-proton collisions at $\sqrt{s} = 13$ TeV with the ATLAS detector," *Phys. Rev. D* **99** (2019) 072001, `arXiv:1811.08856 [hep-ex]`.

[30] ATLAS Collaboration, M. Aaboud et al., "Evidence for the associated production of the Higgs boson and a top quark pair with the ATLAS detector," *Phys. Rev. D* **97** no. 7, (2018) 072003, `arXiv:1712.08891 [hep-ex]`.

[31] ATLAS Collaboration, G. Aad et al., "CP Properties of Higgs Boson Interactions with Top Quarks in the $t\bar{t}H$ and tH Processes Using $H \to \gamma\gamma$ with the ATLAS Detector," *Phys. Rev. Lett.* **125** no. 6, (2020) 061802, `arXiv:2004.04545 [hep-ex]`.

[32] CMS Collaboration, A. M. Sirunyan et al., "Measurements of $t\bar{t}H$ Production and the CP Structure of the Yukawa Interaction between the Higgs Boson and Top Quark in the Diphoton Decay Channel," *Phys. Rev. Lett.* **125** no. 6, (2020) 061801, `arXiv:2003.10866 [hep-ex]`.

[33] ATLAS Collaboration, M. Aaboud et al., "Observation of $H \to b\bar{b}$ decays and VH production with the ATLAS detector," *Phys. Lett. B* **786** (2018) 59–86, `arXiv:1808.08238 [hep-ex]`.

[34] CMS Collaboration, A. M. Sirunyan et al., "Observation of Higgs boson decay to bottom quarks," *Phys. Rev. Lett.* **121** no. 12, (2018) 121801, `arXiv:1808.08242 [hep-ex]`.

[35] ATLAS Collaboration, M. Aaboud et al., "Observation of Higgs boson production in association with a top quark pair at the LHC with the ATLAS detector," *Phys. Lett. B* **784** (2018) 173–191, `arXiv:1806.00425 [hep-ex]`.

[36] CMS Collaboration, A. M. Sirunyan et al., "Observation of $t\bar{t}H$ production," *Phys. Rev. Lett.* **120** no. 23, (2018) 231801, `arXiv:1804.02610 [hep-ex]`.

[37] N. Kauer and G. Passarino, "Inadequacy of zero-width approximation for a light Higgs boson signal," *JHEP* **08** (2012) 116, `arXiv:1206.4803 [hep-ph]`.

[38] F. Caola and K. Melnikov, "Constraining the Higgs boson width with ZZ production at the LHC," *Phys. Rev. D* **88** (2013) 054024, `arXiv:1307.4935 [hep-ph]`.

[39] J. M. Campbell, R. K. Ellis, and C. Williams, "Bounding the Higgs Width at the LHC Using Full Analytic Results for $gg \to e^-e^+\mu^-\mu^+$," *JHEP* **04** (2014) 060, `arXiv:1311.3589 [hep-ph]`.

[40] CMS Collaboration, A. Tumasyan et al., "Measurement of the Higgs boson width and evidence of its off-shell contributions to ZZ production," *Nature Phys.* **18** no. 11, (2022) 1329–1334, `arXiv:2202.06923 [hep-ex]`.

[41] ATLAS Collaboration, G. Aad et al., "Evidence of off-shell Higgs boson production from ZZ leptonic decay channels and constraints on its total width with the ATLAS detector," `arXiv:2304.01532 [hep-ex]`.

[42] CMS Collaboration, "A portrait of the Higgs boson by the CMS experiment ten years after the discovery," *Nature* **607** no. 7917, (2022) 60–68, `arXiv:2207.00043 [hep-ex]`.

[43] ATLAS Collaboration, "A detailed map of Higgs boson interactions by the ATLAS experiment ten years after the discovery," *Nature* **607** no. 7917, (2022) 52–59, `arXiv:2207.00092 [hep-ex]`. [Erratum: Nature 612, E24 (2022)].